Mechanism of current flow and temperature dependence of contact resistivity in Au-Pd-Ti-Pd-n^+-GaN ohmic contacts

A.V. Sachenko[1], A.E. Belyaev[1], N.S. Boltovets[2], L.M. Kapitanchuk[3], V.P. Klad'ko[1], R.V. Konakova[1], A.V. Kuchuk[1], T.V. Korostinskaya[2], A.S. Pilipchuk[4], V.N. Sheremet[1], Yu.I. Mazur[5], M.E. Ware[5], G.J. Salamo[5]
[1]*V. Lashkaryov Institute of Semiconductor Physics, NAS of Ukraine, 03028 Kyiv, Ukraine*
Phone: 38 (044) 525-61-82; Fax: 38 (044) 525-83-42; e-mail: konakova@isp.kiev.ua
[2]*State Enterprise Research Institute "Orion", 03057 Kyiv, Ukraine*
[3]*Paton Institute of Electric Welding, NAS of Ukraine, 03068 Kyiv, Ukraine*
[4]*Institute of Physics, NAS of Ukraine, 03028 Kyiv, Ukraine*
[5]*Department of Physics, University of Arkansas, Fayetteville, Arkansas 72701, USA*

Abstract. We present the results of structural and morphological investigations of interactions between phases in the layers of Au-Pd-Ti-Pd-n^+-GaN contact metallization that appear at rapid thermal annealing (RTA). It is shown that formation of ohmic contact occurs in the course of RTA at $T = 900$ °C due to formation of titanium nitride. We studied experimentally and explained theoretically the temperature dependence of contact resistivity $\rho_c(T)$ of ohmic contacts in the 4.2-380 K temperature range. The $\rho_c(T)$ curve was shown to flatten out in the 4.2-50 K range. As temperature grew, ρ_c decreased exponentially. The results obtained enabled us to conclude that current flow has field nature at saturation of $\rho_c(T)$ and the thermofield nature in the exponential part of $\rho_c(T)$ curve.

Keywords: ohmic contact, temperature dependence of contact resistivity, field mechanism of current flow, thermofield mechanism of current flow.

1. Introduction

It is known that developers of semiconductor devices pin their hopes for production of novel element base for high-temperature-capable electronics on gallium nitride and GaN-based solid solutions [1-7]. Up to now, however, there are no substantial achievements in semiconductor electronics based on wide-gap III–N compounds. The only exception is light-emitting diodes operating at temperatures close to the room one.

The theoretical calculations of AlGaN/GaN-based HEMT [1] and GaN-based Gunn diodes [8] predicted high values of their operating parameters – much over those of similar devices based on GaAs, InP and corresponding solid solutions. Until now, however, the predicted values of HEMT parameters were not obtained experimentally. As to the Gunn diodes, no microwave generation was found with them in the known

experimental works. One of the possible reasons for this (along with the materials science problems and thermal limitations) seems to be ohmic losses [4].

The functional purpose of ohmic contacts is to ensure the required parameters of semiconductor devices operating under preset operating conditions (up to the limiting ones). One of the main prerequisites for error-free performance of semiconductor devices at high temperatures is stability of contact metallization. Since one of GaN components (nitrogen) is volatile, diffusion barriers are needed to prevent active nitrogen transfer (in particular, evaporation) in contact metallization. In addition, diffusion barriers are efficient stoppers for interdiffusion of metallization and semiconductor components [9–11].

The device structures are heated in the course of (i) formation of ohmic contacts at their high-temperature processing and (ii) operation at elevated

temperatures. This leads to a number of physico-chemical processes and structural transformations in contact metallization. As a result, a nonuniform metal-GaN interface appears due to formation of binary, ternary and more complex phases, both extended and localized. These phases lead to transformation and relaxation of intrinsic stresses followed by defect formation in the near-contact region of GaN and the layer forming ohmic contact. This may affect the current flow mechanism in the ohmic contact and consequently the value of contact resistivity ρ_c. Despite a great number of experimental studies, the above processes still remain not adequately understood.

In addition, ohmic contacts (i) must have good adhesion, high electrical and heat conduction, (ii) must demonstrate low chemical reactivity (if possible, be inert) to GaN, (iii) must not form high-resistance junction layers, (iv) must be refractory to stand technological operation modes and limiting operating temperatures, and (v) must not distort interfacial microrelief. It is very difficult (or even impossible) to meet the above requirements.

It was shown in some recent experimental works on ohmic contacts to GaN that intrinsic stresses appear in the near-contact region of GaN because of mismatch between the coefficients of thermal expansion and lattice constants of semiconductor and metal. These intrinsic stresses relax as contact metallization is cooled, with appearance of high density of structural defects, in particular, dislocations. Their density, along with that of growth dislocations in GaN grown on foreign substrates (Al_2O_3, SiC, GaAs, Si), exceeds 10^8 cm^{-2}. Growth of contact resistivity ρ_c with temperature was observed in ohmic contacts with the above density of structural defects in the near-contact region of n-GaN $[12-21]$.

In some works [19-21], growth of ρ_c with temperature was observed within the range of operating temperatures for gallium nitride devices (~20 to 500 °C). Some authors [12-15] relate such a behavior of ρ_c directly with a high density of structural defects, in particular, dislocations (both growth ones and those appearing in the course of manufacturing the ohmic contacts In-GaN (GaP)). The authors of [12-14] assumed that, in such a spatially-nonuniform medium, dislocations serve as formation centers for metal shunts that appear because of transfer of metal from the contact metallization over dislocations. However, this model explains the linear growth of ρ_c with temperature only, as it should be in the case of metallic conduction.

At the same time, more complicated nonmonotonic dependences $\rho_c(T)$ were observed experimentally (along with linear ones). They were explained in [16-18] whose authors assumed, using a model of metal shunts, that an accumulation layer (instead of the traditional depletion one) may appear in the semiconductor region adjacent to the shunt end. The calculations showed that allowance for that factor, along with limitation of current flowing through the metal shunts by diffusion supply of electrons, makes it possible to describe the experimental

temperature dependences $\rho_c(T)$, both growing and decreasing with temperature.

There are a number of experimental works dealing with the mechanisms of current flow in ohmic contacts to n-GaN, with allowance made for the temperature dependence of their contact resistivity. They describe the features of temperature dependence of ρ_c in the temperature ranges 293-773 K [19-21] and 100-450 K [12-18, 22, 23]. At the same time, there are practically no studies of $\rho_c(T)$ behavior in the 4-100 K temperature range, although they would be of importance for determination of current flow mechanisms in ohmic contacts to wide-gap III−N semiconductors.

In this work, we investigated the formation mechanisms for ohmic contacts to n^+-n-n^+-GaN structure and mechanism of current flow in it within the 4.2-380 K temperature range. To make that contact, we applied the thin-film multilayer contact system Au–Pd–Ti–Pd .

2. Specimens and methods of investigation

We investigated the specimens of two types based on the n^+-n-n^+-GaN structures: (i) test structures for measurement of phase and elemental composition of specimens with continuous metallization layer and (ii) test structures for measurement of temperature dependence of contact resistivity ρ_c. The n^+-n-n^+-GaN films were prepared on sapphire using plasma-assisted molecular beam epitaxy (PAMBE) at the temperature 800 °C. The n^+-layers were doped with silicon up to concentration ~2.7·10^{18} cm^{-3}, the thicknesses of buffer layer, upper cap layer and undoped n-layer were 4 μm, ~1 μm and ~2 μm, respectively [24].

The layers Pd(30 nm)-Ti(60 nm)-Pd(50 nm)-Au(50 nm) were applied onto a substrate heated to 300 °C using thermal vacuum deposition. The phase composition of contact metallization was measured using X-ray diffraction (XRD), with an X-ray diffractometer Philips X'Pert MRD (Cu$_{K\alpha}$-line, $\lambda = 0.15418$ nm) in the Bragg-Brentano geometry, before and after rapid thermal annealing (RTA) in vacuum (pressure 10^{-4} Pa) at temperatures 700 and 900 °C for 30 s.

The concentration depth profiles of elements in the ohmic contacts were taken with Auger Microprobe JEOL JAMP 9500F equipped with an INCA Penta FETx3 energy dispersive spectrometer (Oxford Instruments). Layer-by-layer elemental analysis was made using etching the surface of the specimen studied with Ar$^+$ ions (energy 3 keV).

We determined chemical compounds in the metal layers of ohmic contacts by applying the software "Spectra investigator" (JEOL) and deconvolution of the Auger spectra, using the spectra of standard specimens (Ti, TiO_2, TiC, TiN, TiB_2).

The temperature dependence of contact resistivity in packaged specimens was measured within the 4.2-380 K temperature range with the transmission line method [25]. The temperature control was performed
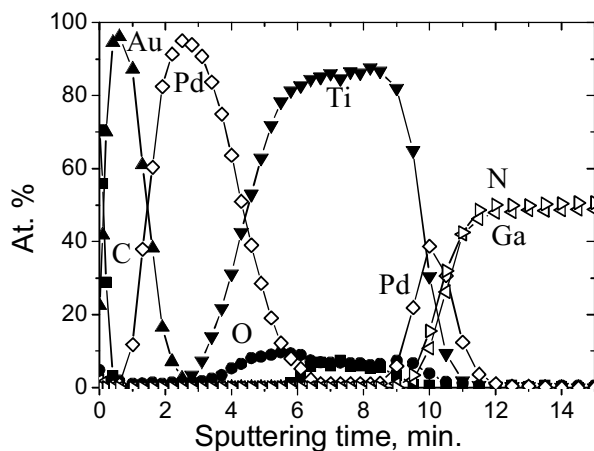
with two thermoresistive sensors. Temperature was stabilized with an УТРЕКС К25в system: for temperatures below 30 K, at a level no worse than 0.05 K; for the range 30-100 K, no worse than 0.1 K; for temperatures over 100 K, at the level 0.5 K.

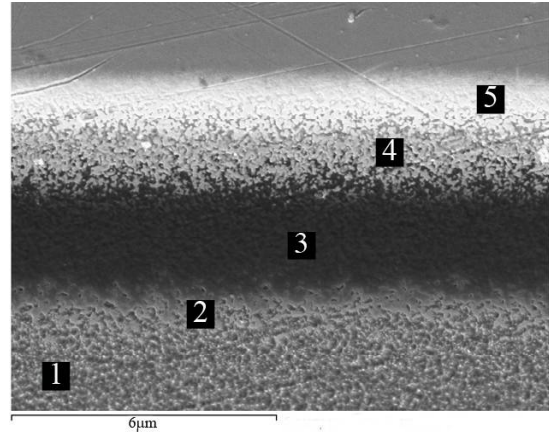## 3. Structural and morphological studies of contact metallization

The results of Auger electron spectroscopy (Fig. 1) and analysis of elemental composition at oblique cut of metallization (Fig. 2) showed that metallization in the initial specimen has layer structure with some smearing of concentration depth profiles near the corresponding interfaces Au-Pd, Pd-Ti, Ti-Pd. The titanium film contains up to 6-8% oxygen and 6% carbon (Fig. 1). An analysis of chemical composition near the contact forming layer-GaN interface showed that titanium penetrates through palladium film into GaN (see Figs 1, 2 and Table 1). Judging from the results of deconvolution of the Auger spectra of titanium (region of etching for 2-11 min, see Figs 1, 3), the traces of titanium nitride are observed over the whole film thickness. This indicates a possibility of titanium nitridization already in the course of metallization layers deposition onto the substrate heated to 300 °C.

**Table 1. Elemental composition of five local areas at a cut of Au-Pd-Ti-Pd-n^+-GaN contact.**

| #	Atomic %						
	C	N	O	Ti	Ga	Pd	Au
1	2.76	48.64	1.37	0.06	46.48	0.00	0.19
2	5.04	46.99	1.12	0.00	45.30	1.56	0.00
3	5.74	38.72	1.01	7.97	41.60	4.96	0.00
4	8.21	28.83	0.00	18.25	31.36	13.35	0.00
5	11.32	19.54	0.00	13.45	14.21	22.77	12.71

Fig. 2. Oblique cut of Au-Pd-Ti-Pd-n^+-GaN contact metallization (initial specimen). (The elemental composition of five local areas has been presented in Table 1.)
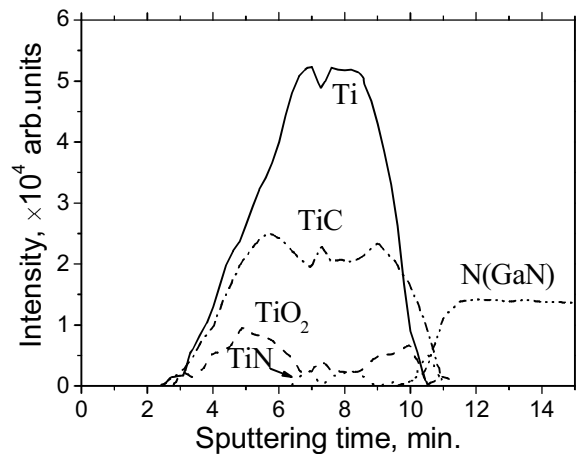
Fig. 3. Concentration depth profiles of Ti, TiC, TiO$_2$ and TiN in Au-Pd-Ti-Pd-n^+-GaN contact metallization for the initial specimen (obtained by deconvolution of Auger spectra of titanium).

RTA at $T = 700$ °C breaks the layer structure of contact metallization (Fig. 4) and leads to intensification of the process of titanium nitride formation near the Pd-GaN interface. Taking into account the results of formation of Ti-based ohmic contact to *n*-GaN [3, 4, 10, 11, 26, 27] and in accordance with the data given in [28], one may suppose that the following reactions are predominant in the physico-chemical process under consideration:

$$Ti + GaN \rightarrow TiN_x + GaN_{1-x},$$

$$2Ti + Pd \rightarrow PdTi_2.$$
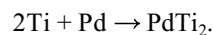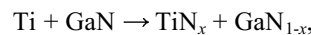
The results of deconvolution of the titanium Auger spectra (see Fig. 5) indicate also a possibility of TiC and TiO$_2$ formation practically over the whole region of intermixing occupied by titanium. Intermixing of metallization components is supported also by the oblique cut of metallization layers (Fig. 6a) and Auger spectra at the areas 1-7 in different regions of the cut (Fig. 6b).
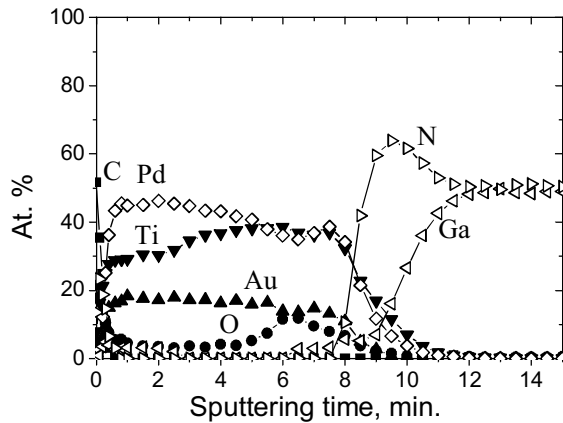

Fig. 1. Concentration depth profiles for Au-Pd-Ti-Pd-n^+-GaN contact metallization (initial specimen has been prepared using metal deposition onto the substrate heated to 300 C).

Fig. 4. Concentration depth profiles for Au-Pd-Ti-Pd-n^+-GaN contact metallization after RTA at $T = 700$ °C.
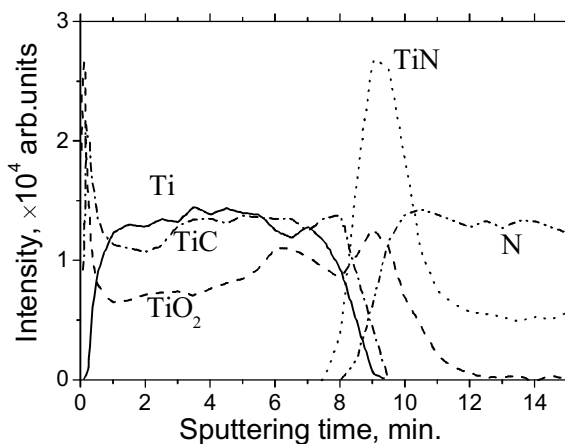

Fig. 5. Concentration depth profiles of Ti, TiC, TiO_2 and TiN in Au-Pd-Ti-Pd-n^+-GaN contact metallization after RTA at $T = 700$ °C (obtained by deconvolution of Auger spectra of titanium).

RTA at $T = 900$ °C leads to decomposition of GaN [2, 3] and penetration of semiconductor atoms to the outer metallization surface with content of gallium up to 2 atomic % and nitrogen ~14%, as well as titanium up to 10% at the surface and up to 20% in the near-surface layer (Figs 7a, 7b). An intense mass transfer of titanium to GaN is observed at the inner intermixing region-GaN interface (Fig. 7a). The character of atomic profiles of nitrogen and titanium in the GaN near-contact region indicates formation of titanium nitride in it. This is supported also by the results of deconvolution of titanium spectra for the specimen considered (Fig. 8) that indicate predominance of TiN (as compared with TiO_2 and TiC) in the ohmic contact region. It follows from the above data that just titanium nitride forms ohmic contact to n-GaN.

It should be also noted that the surface morphology of the upper metallization layers and metal-GaN interface correlates with the concentration depth profiles of metallization components after RTA at $T = 900$ °C (Figs 9 and 10, respectively). Indeed, after RTA the unetched Au film is not continuous. One can see this

from Fig. 9 and analysis of elemental composition in four local areas of surface (Fig. 9 and Table 2). All the components of contact metallization and semiconductor are observed in different surface areas, with a higher content of titanium and palladium where the gold film is broken and lower content of titanium and palladium where the gold film is continuous. This indicates the high degree of metallization layers intermixing as well as possibility of formation of phases containing titanium and palladium, in accordance with the high-temperature phase diagram Pd – Ti [29], say, according to the reaction $PdTi_2 + 5Pd \rightarrow 2Pd_3Ti$.
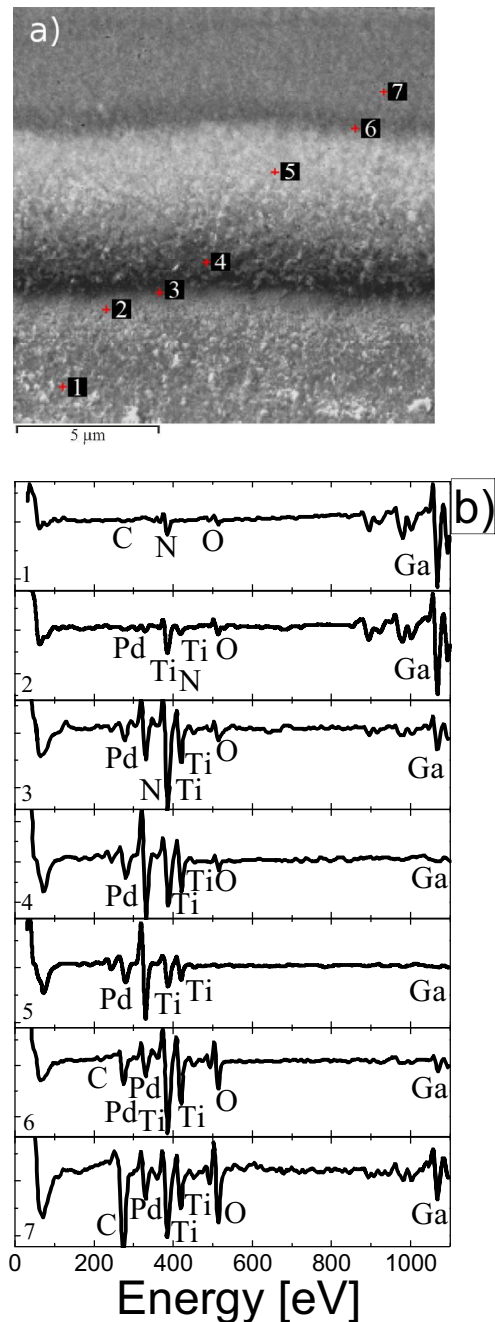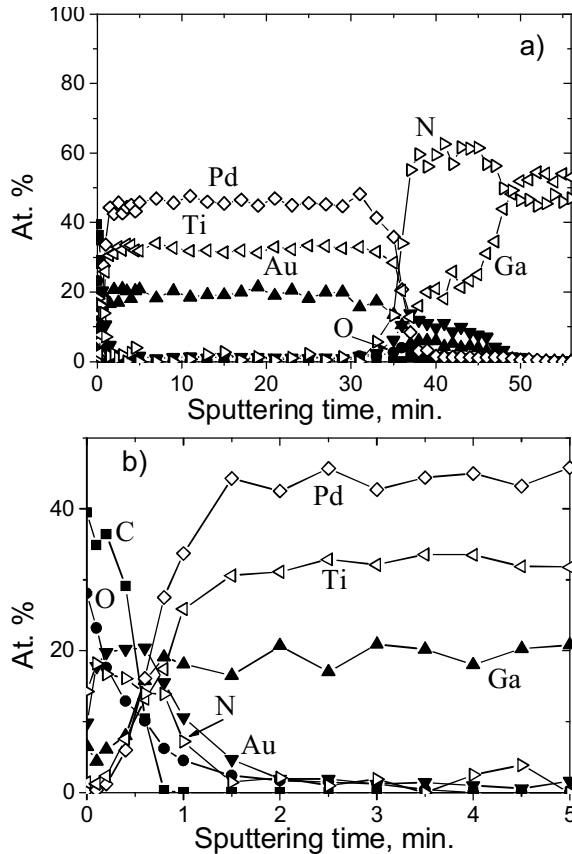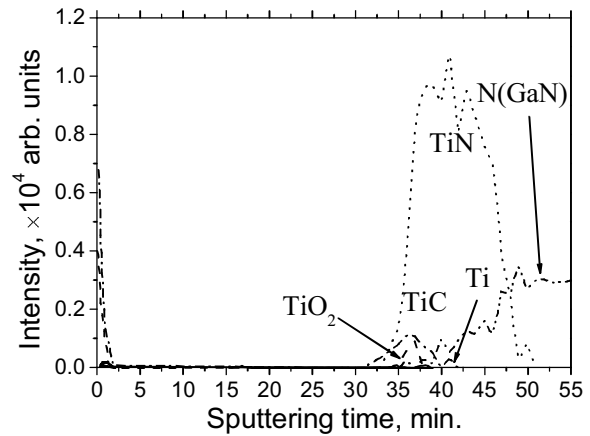

Fig. 6. a) oblique cut of Au-Pd-Ti-Pd-n^+-GaN contact metallization after RTA at $T = 700$ °C; b) Auger spectra measured at the local areas 1-7 indicated in Fig. 6a.
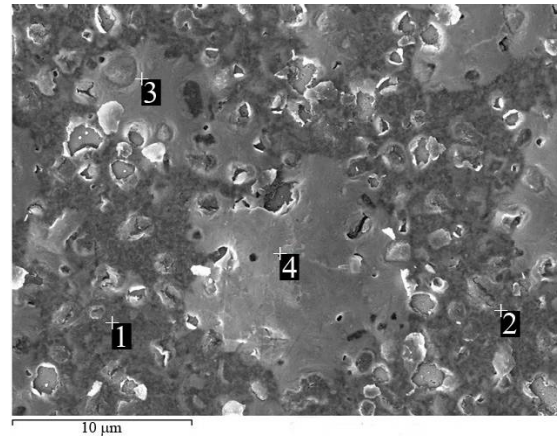
Fig. 7. Concentration depth profiles for Au-Pd-Ti-Pd-n^+-GaN contact metallization after RTA at $T = 900$ °C: a) over the whole metallization thickness; b) in the near-surface region at the outer surface of metallization.

Fig. 8. Concentration depth profiles of Ti, TiC, TiO_2 and TiN in Au-Pd-Ti-Pd-n^+-GaN contact metallization after RTA at $T = 900$ °C (obtained by deconvolution of Auger spectra of titanium).

Fig. 9. Morphology of unetched Au film after RTA at $T = 900$ °C. (The elemental composition of four local areas is presented in Table 2.)

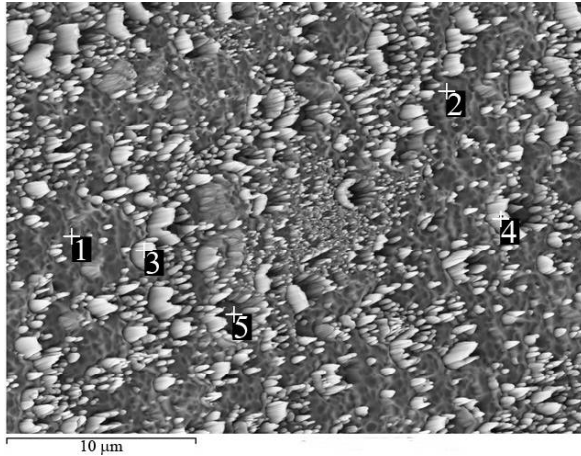**Table 2. Elemental composition of four local areas at Au film surface after RTA at $T = 900$ °C.**

#	Atomic %						
	C	N	O	Ti	Ga	Pd	Au
1	11.24	28.13	4.39	10.26	35.99	5.10	4.89
2	12.43	28.43	4.62	12.84	31.96	4.91	4.81
3	15.04	1.72	3.10	2.07	25.17	35.42	17.47
4	19.19	2.59	4.98	3.90	21.84	32.13	15.36

Table 3. Elemental composition of five local areas at GaN surface after RTA at $T = 900$ °C (metallization layers removed).

#	Atomic %						
	C	N	O	Ti	Ga	Pd	Au
1	0.00	48.17	1.23	0.19	50.41	0.00	0.00
2	2.41	47.91	1.26	0.58	47.81	0.00	0.03
3	0.00	48.26	0.84	0.00	50.90	0.00	0.00
4	8.31	49.20	1.31	0.00	41.04	0.00	0.15
5	1.32	50.75	0.31	0.00	47.51	0.00	0.10

As to the GaN surface morphology after removal of metallization by etching of the specimen subjected to RTA at 900 °C, one can see from Fig. 10 that it is characterized by a developed microrelief. The surface analyzed contains small amount of titanium (local areas 1 and 2 in Fig. 10 and Table 3), and gold (local area 5 in Fig. 10 and Table 3) (which indicates mass transfer in the contact metallization) and small amounts of carbon and oxygen (see the corresponding local areas 1-5 in Fig. 10 and Table 3). A similar structure of metallization layers and GaN surface can be seen rather clearly at the oblique cut of that specimen (Fig. 11, local areas 1-5 in Table 4). One can see that the GaN surface is of the same type as in the previous figure (local area 1 in Fig. 10 and Table 3). Presence of titanium, palladium and gold was detected in the GaN near-contact region (local area 2 in Fig. 11 and Table 4). The palladium and gold content grows considerably when going at the contact cut to the upper metallization layer (local areas 3-5 in Fig. 11 and Table 4). Judging from the concentration depth profiles of contact metallization components (Fig. 7a), this characterizes the intermixing region that occupies practically whole metallization thickness.

Fig. 10. Morphology of GaN surface after removal of metallization by using ion etching and subjection of the specimen to RTA at $T = 900$ °C. (The elemental composition of five local areas has been presented in Table 3.)
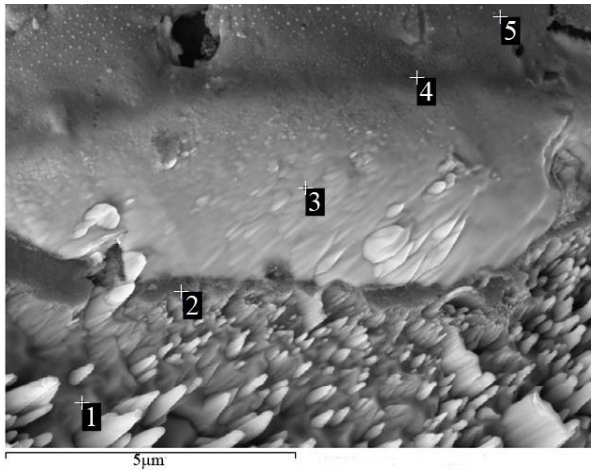
Fig. 11. Oblique cut of Au-Pd-Ti-Pd-n^+-GaN contact metallization after RTA at $T = 900$ °C. (The elemental composition of five local areas has been presented in Table 4.)

Table 4. Elemental composition of five local areas at cut of contact metallization after RTA at $T = 900$ °C.

#	Atomic %						
	C	N	O	Ti	Ga	Pd	Au
1	7.88	49.37	0.23	0.40	42.06	0.00	0.06
2	0.00	52.58	0.00	2.97	43.47	0.52	0.46
3	0.00	16.50	0.00	0.00	30.30	36.44	16.76
4	0.00	10.52	3.14	3.02	26.85	37.59	19.15
5	0.00	2.96	6.28	3.00	31.50	37.99	18.27

The phase composition of the Au-Pd-Ti-Pd-n-GaN contact metallization for the initial specimen and that subjected to RTA at $T = 700$ °C (900 °C) are presented in Fig. 12 (curves 1, 2 and 3, respectively). One can see that the XRD pattern of the initial specimen contains reflections Au (111) and Pd (111) from strongly textured metal layers. Since the reflections from the titanium film

are close to those of gold and palladium, it was impossible to determine the structure of the titanium film. Formation of the $PdTi_2$ phase was detected after RTA at $T = 700$ °C, so it seems that titanium in the initial specimen is most probably in X-ray amorphous state. The fact that no reflections from pure palladium and titanium were detected after RTA at $T = 700$ °C indicates their complete intermixing. Only slight shift of the gold peak was detected. This seems to be related to diffusion of palladium and titanium atoms to the gold film. Formation of the Pd_3Ti phase and nonstoichiometric phases of the Au_xGa (Pd, Ti) solid solutions were observed in the specimens subjected to RTA at $T = 900$ °C.

Thus, one can conclude from the above data on the elemental and phase composition of contact metallization that a thin layer of titanium nitride is formed near the contact forming layer–GaN interface. Just this layer determines the contact ohmicity. As to the efficiency of diffusion barriers, judging from our previous works [9, 28], it is possible to increase it by using a thin film of amorphous TiB_2 as diffusion barrier that does not interact (up to $T = 900$ C) with either the metallization components or GaN.
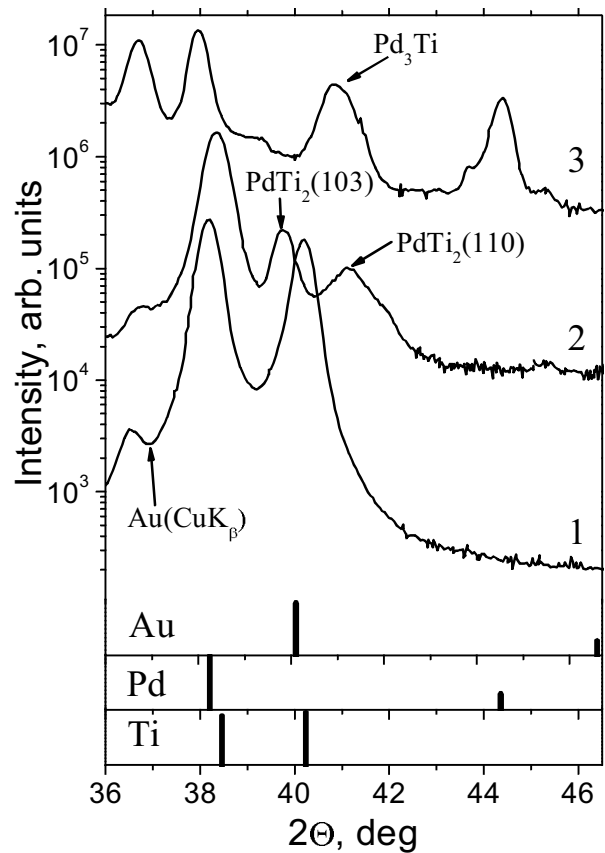
Fig. 12. XRD patterns of Au-Pd-Ti-Pd-n^+-GaN contact metallization: 1) initial specimen; 2) after RTA at $T = 700$ °C; 3) after RTA at $T = 900$ °C.

4. Electrical characteristics of Au-Pd-Ti-Pd-GaN ohmic contacts

The *I−V* curves of ohmic contacts taken before and after RTA at *T* = 700 °C (900 °C) were linear. At room temperature, the initial specimens and those subjected to RTA at *T* = 700 °C demonstrated rather high contact resistivity (ρ_c = 2…3 $\Omega \cdot \text{cm}^2$ in the initial specimen and ~0.3 $\Omega \cdot \text{cm}^2$ in that after RTA at *T* = 700 °C). After RTA at *T* = 900 °C, ρ_c decreased considerably and was ~ $6 \cdot 10^{-4} \ldots 10^{-3} \, \Omega \cdot \text{cm}^2$ at room temperature.

The typical temperature dependence of ρ_c measured in the 4.2-380 K temperature range is presented in Fig. 13. One can see that the $\rho_c(T)$ curves flattens out at temperatures below 50 K. In this case, the pure field mechanism of current flow takes place because of high degeneracy of semiconductor in the near-contact region and pure electron tunneling through the barrier. The tunnel current near *T* = 0 K is described by the expression obtained in [30]. One should note that, as $T \to 0$, the tunnel current density J_{FE} may be written as

$$J_{FE} = qN_d V_{TO} \left[\exp\left(-\frac{\varphi_b - E_{F\,\text{lim}} - qV}{E_{00}} \right) - \exp\left(-\frac{\varphi_b - E_{F\,\text{lim}}}{E_{00}} \right) \right]. \qquad (1)$$

Here, *q* is the elementary charge, N_d − shallow donor concentration (to which the electron concentration is equal), $V_{TO} = q^2 / \hbar \varepsilon_0 \varepsilon_s K^2$ − rate of electron supply to the contact, K = log$[4(\varphi_b - E_{F\,\text{lim}})/ E_{F\,\text{lim}}]$ − coefficient of the order of unity, $E_{F\,\text{lim}} = \left(3\pi^2\right)^{2/3} \hbar^2 N_d^{2/3} / 2m_n^*$ − limiting Fermi energy in the case of high degeneracy [31], $\hbar$ − Planck constant, m_n^* − electron effective mass, φ_b − electron potential energy, i.e., barrier height, $E_{00} = 0.054\left((m_0 / m^*)(N_d /10^{20}\,\text{cm}^{-3})(11.7 / \varepsilon_s)\right)^{0.5}$ − characteristic tunneling energy (in eV), *V* − applied voltage, ε_s − semiconductor permittivity.
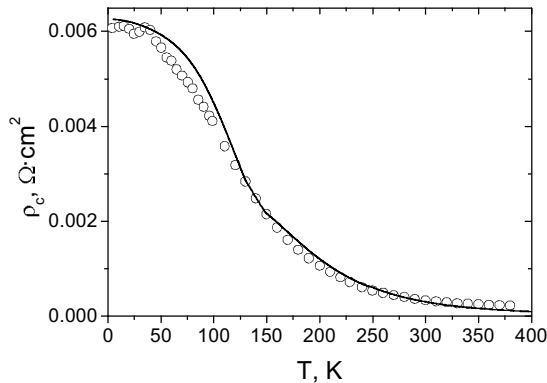
Fig. 13. Temperature dependence of contact resistivity $\rho_c(T)$ in the Au-Pd-Ti-Pd-n^+-GaN contact system after RTA at *T* = 900 °C: open circles − experiment, solid curve − theoretical calculation.

At temperatures over zero, Eq. (1) takes a look:

$$J_{FE}(T) = qN_d V_T(T) \left[\exp\left(-\frac{\varphi_b - E_F(T) - qV}{E_0(T)} \right) - \exp\left(-\frac{\varphi_b - E_F(T)}{E_0(T)} \right) \right], \qquad (2)$$

where $V_T(T) = 2\pi A \left(m_n^* / m_0 \right) T E_{00} / \left(\kappa kT \sin\left(\kappa \pi kT / 2E_{00} \right) qN_d \right)$, $E_0 = E_{00} \coth\left(E_{00} / kT \right)$, E_F is the Fermi energy, *A* − Richardson constant.

The expression for temperature dependence of tunnel contact resistivity $\rho_c(T)$ is obtained by differentiating the tunnel current density (Eq. (2)) with respect to the applied bias:

$$\rho_c(T) = \frac{E_0(T)}{q^2 N_d V_T(T)} \left[\exp\left(\frac{\varphi_b - E_F}{E_0(T)} \right) \right], \qquad (3)$$

At higher temperatures, current flow is determined by the thermofield mechanism, and $\rho_c(T)$ is given by the corresponding expression from [32]:

$$\rho_{TF} = \frac{k\sqrt{E_{00}} \cosh\left(E_{00} / kT \right) \coth\left(E_{00} / kT \right)}{A\left(m^* / m_0 \right) T \, q\sqrt{\pi(\varphi_b - E_F)}} \times$$
$$\times \exp\left[\frac{\varphi_b - E_F}{E_{00} \coth\left(E_{00} / kT \right)} + \frac{E_F}{kT} \right]. \qquad (4)$$

The temperature dependence $E_F(T)$ can be found from the equation of electrical neutrality of semiconductor

$$N_d = n = \frac{2}{\sqrt{\pi}} N_c \left(\frac{T}{300} \right)^{3/2} \int_0^\infty \frac{x^{0.5}}{1 + \exp(x - \varepsilon_F)} dx, \qquad (5)$$

where N_c is the effective density of states in the conduction band at *T* = 300 K, $\varepsilon_F(T) = E_F(T)/kT$.

The theoretical curve in Fig. 13 is plotted using Eq. (3) within the 4.2-130 K temperature range and Eq. (4) within the 130-380 K temperature range. One can see a rather good agreement between the theoretical and experimental $\rho_c(T)$ curves.

5. Conclusion

The measurements of temperature dependence of contact resistivity $\rho_c(T)$ for the Au-Pd-Ti-Pd-n^+-GaN structure with the impurity concentration $3 \cdot 10^{18}\,\text{cm}^{-3}$ within the 4.2-380 K temperature range showed that there is a portion of $\rho_c(T)$ curve independent of temperature in the 4.2-50 K temperature range. The pure tunnel mechanism of current flow is realized in this portion. At higher temperatures, $\rho_c(T)$ is decreased with temperature, and the main mechanism of current flow here is thermofield emission.

It is found that, owing to RTA at $T = 900$ °C for 30 s, titanium nitride is formed in the near-contact region of GaN in the Au-Pd-Ti-Pd-n^+-GaN contact metallization, besides Pd_3Ti phase and nonstoichiometric phase of Au_xGa (Pd, Ti) solid solution. This titanium nitride forms an ohmic contact.

Acknowledgements

References

1. M.S. Shur, GaN based transistors for high power applications // *Solid State Electron.* **42**(12), p. 2131-2168 (1998).
2. Yu.G. Shreter, Yu.T. Rebane, V.A. Zykov, V.G. Sidorov, *Wide-Gap Semiconductors*. Nauka, Sankt-Peterburg, 2001 (in Russian).
3. V.N. Danilin, Yu.P. Dokuchaev, T.A. Zhukova M.A. Komarov, Power high-temperature-capable and radiation-resistant new-generation microwave devices with wide-gap AlGaN/GaN heterojunction structures // *Obzory po Elektronnoi Tekhnike*, Ser. 1. SVCh Tekhnika, GUPNPP "Pulsar", Moscow, 2001 (in Russian).
4. Yu.V. Kolkovskii, Yu.A. Kontsevoi, A.G. Vasil'ev, *Microwave Wide-Gap Semiconductor Transistors*. Teknosfera, Moscow, 2011 (in Russian).
5. R. Quay, *Gallium Nitride Electronics*. Springer-Verlag, Berlin, Heidelberg, 2008.
6. H. Morkoç, *Handbook of Nitride Semiconductors and Devices*: *Materials Properties, Physics and Growth*, Vol. 1. Wiley-VCH Verlag GmbH&Co KGaA, Weinheim, 2008.
7. *Nitride Semiconductors: Handbook of Materials and Devices*, P. Ruterana, M. Albrecht, J. Neugebauer (Eds.). Wiley-VCH Verlag GmbH&Co KGaA, Weinheim, 2003.
8. Yu.V. Arkusha, E.D. Prokhorov, I.P. Storozhenko, Power and frequency characteristics of Gunn-diodes on the basis of GaN // *Proc. 15th Intern. Crimean Conf. "Microwave Telecommunication Technology" (CriMiCo'2005)*, 12-16 Sept., Sevastopol, Crimea, Ukraine, **1**, p. 166 (2005).
9. A.E. Belyaev, N.S. Boltovets, R.V. Konakova, V.V. Milenin, Ya.Ya. Kudryk, Diffusion barriers in ohmic contacts to semiconductor device structures: Technology. Properties. Application, in: *Adv. in Mater. Sci. Res*. **12** / Ed. Maryam C. Wytters, Nova Publ., N.Y. (2012).
10. S. Noor Mohammad, Contact mechanisms and design principles for alloyed ohmic contacts to *n*-GaN // *J. Appl. Phys.* **95**(12), p. 7940-7953 (2004).
11. Liang Wang, Fitih M. Mohammad, Ilesanmi Adesida, Formation mechanisms of ohmic contacts on AlGaN/GaN heterostructure: Electrical and microstructural characterizations // *J. Appl. Phys.* **103**(9), 093516 (2008).
12. T.V. Blank, Yu.A. Gol'dberg, O.V. Konstantinov, V.G. Nikitin, E.A. Posse, The mechanism of current flow in an alloyed In-GaN ohmic contact // *Semiconductors*, **40**(10), p. 1173-1177 (2006).
13. T.V. Blank, Yu.A. Gol'dberg, Mechanisms of current flow in metal-semiconductor ohmic contacts // *Semiconductors*, **41**(11), p. 1263-1292 (2007).
14. V.N. Bessolov, T.V. Blank, Yu.A. Gol'dberg, O.V. Konstantinov, E.A. Posse, Dependence of the mechanism of current flow in the In-*n*-GaN alloyed ohmic contact on the majority carrier concentration // *Semiconductors*, **42**(11), p. 1315-1317 (2008).
15. T.V. Blank, Yu.A. Gol'dberg, E.A. Posse, Flow of the current along metallic shunts in ohmic contacts to wide-gap III−V semiconductors // *Semiconductors*, **43**(9), p. 1164-1169 (2009).
16. A.V. Sachenko, Formation mechanisms of contact resistance of metal-semiconductor ohmic contacts, in: *Physical Diagnostic Methods in Micro- and Nanoelectronics*, A.E. Belyaev, R.V. Konakova (Eds.), p. 281-346, ISMA, Kharkov, 2011 (in Russian).
17. A.V. Sachenko, A.E. Belyaev, A.V. Bobyl, N.S. Boltovets, V.N. Ivanov, L.M. Kapitanchuk, R.V. Konakova, Ya.Ya. Kudryk, V.V. Milenin, S.V. Novitskii, D.A. Sakseev, I.S. Tarasov, V.N. Sheremet, M.A. Yagovkina, Temperature dependence of the contact resistance of ohmic contacts to III−V compounds with a high dislocation density // *Semiconductors*, **46**(3), p. 334-341 (2012).
18. A.V. Sachenko, A.E. Belyaev, N.S. Boltovets, R.V. Konakova, Ya.Ya. Kudryk, S.V. Novitskii, V.N. Sheremet, J. Li, S.A. Vitusevich, Mechanism of contact resistance formation in ohmic contacts with high dislocation density // *J. Appl. Phys.* **111**(8), 083701 (2012).
19. Changzhi Lu, Hongnai Chen, Xiaoliang Lv, Xuesong Xie, S. Noor Mohammad, Temperature and doping-dependent resistivity of Ti/Au/Pd/Au multilayer ohmic contact to *n*-GaN // *J. Appl. Phys.* **91**(11), p. 9218-9224 (2002).
20. Zhang Yuesong, Feng Shiwei, Zhang Gongchang, Wang Chengdong, Lu Changzhi, High temperature characteristics of Ti/Al/Ni/Au multilayer ohmic contacts to *n*-GaN // *Chin. J. Semicond.* **28**(6), p. 984-988 (2007).
21. Zhang Yue-Zong, Feng Shi-Wei, Guo Chun-Sheng, Zhang Guang-Chen, Zhuang Si-Xiang, Su Rong, Bai Yun-Xia, Lu Chang-Zhi, High temperature characteristics of Ti/Al/Ni/Au ohmic contacts to *n*-GaN // *Chin. Phys. Lett.* **25**(11), p. 4083-4085 (2008).
22. Rohit Khanna, Development of high temperature stable ohmic and Schottky contacts to *n*-GaN. *A dissertation* presented to the graduate school of the Univ. of Florida in partial fulfillment of the

requirements for the Degree of Doctor of Philosophy, Univ. of Florida (2007).

23. Lars Frederik Voss, Thermally stable ohmic and Schottky contacts to GaN. *A dissertation* presented to the graduate school of the Univ. of Florida in partial fulfillment of the requirements for the Degree of Doctor of Philosophy, Univ. of Florida (2008).

24. V.V. Strelchuk, V.P. Bryksa, K.A. Avramenko, M.Ya. Valakh, A.E. Belyaev, Yu.I. Mazur, M.E. Ware, E.A. DeCuir Jr., G.J. Salamo, Confocal Raman depth-profile analysis of the electrical and structural properties in III-nitride structures // *Phys. Status Solidi* (*c*), **8**(7-8), p. 2188-2190 (2011).

25. D.K. Schroder, *Semiconductor Materials and Devices Characterization*. Wiley, N.Y., 2006.

26. A.G. Vasil'ev, Yu.V. Kolkovskii, Yu.A. Kontsevoi, *Microwave Wide-Gap Semiconductor Devices and Facilities*. Teknosfera, Moscow, 2011 (in Russian).

27. S. J. Pearton, *Processing of Wide Band Gap Semiconductors.* Noyes Publ., N.Y., 2000.

28. A.E. Belyaev, N.S. Boltovets, V.N. Ivanov, R.V. Konakova, Ya.Ya. Kudryk, P.M. Lytvyn, V.V. Milenin, Yu.N. Sveshnikov, Thermal stability of multilayer contacts on gallium nitride // *Techn. Phys Lett.* **31**(12), p. 1078-1081 (2005).

29. R.P. Elliott, *Constitution of Binary Alloys. First Supplement*. McGraw-Hill, New York, 1965.

30. F.A. Padovani, R. Stratton, Field and thermionic-field emission in Schottky barriers // *Solid State Electron*. **9**(7), p. 695-707 (1966).

31. V.L. Bonch-Bruevich, S.G. Kalashnikov, *Physics of Semiconductors*, 2nd Ed. Nauka, Moscow, 1990 (in Russian).

32. S.M. Sze, K. Ng. Kwok, *Physics of Semiconductor Devices.* John Wiley & Sons Inc. Publ., 2007.